Measurement Science and Technology

PAPER

Check for updates

OPEN ACCESS

RECEIVED
3 April 2026

REVISED
9 June 2026

ACCEPTED FOR PUBLICATION
23 June 2026

PUBLISHED
14 July 2026

Multiconductor transmission line model for induced stray-currents due to railway systems on ground buried structures

Lino Di Leonardo[1], **Francesco de Paulis**[2,*], **Antonio Orlandi**[2], **Fabio Sbarra**[3] **and Marco Camomilla**[3]

[1] Department of Industrial Engineering, University of Padua, 35131 Padova, Italy
[2] Department of Industrial and Information Engineering and Economics, University of L'Aquila, 67100 L'Aquila, Italy
[3] RFI R&D, 00161 Rome, Italy
[*] Authors to whom any correspondence should be addressed.

E-mail: lino.dileonardo@unipd.it, francesco.depaulis@univaq.it, antonio.orlandi@univaq.it, f.sbarra@rfi.it and m.camomilla@rfi.it

Keywords: stray-current, DC-electrified railway, rail voltage, DC traction

Abstract

Stray currents generated by electrified railway systems represent a significant source of interference and long-term degradation for ground-embedded metallic structures, including pipelines, reinforcing bars, cable sheaths, and utility networks. Accurate prediction of current distribution and induced potentials is therefore essential for assessing corrosion risk and system reliability. This paper presents a comprehensive multiconductor transmission line model for analyzing induced stray currents on buried structures in the presence of railway traction systems. The proposed formulation treats rails and nearby metallic infrastructures as electromagnetically coupled conductors within a unified framework. The governing equations are derived from the generalized telegrapher's equations, incorporating longitudinal impedance, transverse admittance, soil resistivity, and mutual coupling effects. The model enables the computation of distributed voltages and currents along extended structures under the train operating condition. Attention is devoted to the coupling mechanisms between traction return currents and adjacent buried conductors, highlighting the influence of soil parameters and electrical bonding conditions. Numerical simulations demonstrate the approach's ability to predict current leakage profiles and potential gradients. Validation is demonstrated by comparing the computed results with those obtained by alternative circuit models and measurements. The results provide valuable insights for corrosion risk assessment, the design of mitigation strategies, and regulatory compliance in railway environments.

1. Introduction

Railway transportation represents a cornerstone of modern mobility systems, enabling the efficient movement of passengers and freight across extensive rail networks. The progressive electrification of railway infrastructures—introduced to improve operational efficiency and environmental sustainability—has also led to new technical challenges. Among these, the phenomenon of stray current has emerged as a significant concern for railway operators and infrastructure managers.

Stray currents are unintended electrical currents that deviate from their designated return paths and propagate through surrounding conductive media, such as soil or nearby metallic structures. These currents originate from the interaction between electrified railway systems and the surrounding environment. Their presence can cause several adverse effects, including accelerated corrosion of buried metallic assets, disruptions to signaling and communication systems, and potential safety risks to railway operations. In DC electrified railway systems, stray current leakage is expected in areas close to the tracks; consequently, mitigation and protection measures are typically implemented for vulnerable installations such as buried pipelines and other metallic infrastructures [1, 2].

A key parameter governing the generation and propagation of stray currents is the rail potential, commonly referred to as rail voltage (V_r). This quantity represents the main driving force for current leakage from the rails into the surrounding environment. Rail voltage is influenced by several factors, including the traction power supply configuration, the electrical characteristics of the track structure, and soil properties. The interactions among these elements determine both the magnitude and the spatial distribution of stray currents along railway lines. Therefore, a detailed understanding of these relationships is essential for developing effective strategies to mitigate the associated risks [3–5].

Over the past few decades, considerable research effort has been devoted to investigating stray-current phenomena in railway systems. These studies include both theoretical analyses and experimental investigations aimed at clarifying the mechanisms governing current leakage and identifying appropriate monitoring and mitigation techniques. For instance, previous work has reviewed the main electrical quantities associated with stray current phenomena, as well as protection strategies and corrosion mechanisms. Such quantities are fundamental for implementing stray current monitoring systems, which provide indicators of the overall health of the traction return circuit. The literature also discusses operational conditions of railway systems, criteria for stray-current protection systems, measurement techniques, and the functional requirements of monitoring systems, and proposes procedures to assess their reliability through simulated leakage scenarios [6].

The development of accurate simulation environments is crucial for studying stray current behavior. By reproducing realistic operating conditions—such as rail voltage profiles and environmental parameters—simulation models allow researchers to investigate the phenomenon under controlled conditions and to evaluate mitigation strategies during the early stages of design and infrastructure development. Moreover, simulation frameworks provide a safe platform for experimentation, reducing the need for intrusive tests on operating railway networks [7].

Several contributions in the literature have addressed the numerical modeling of stray current distribution in electrified railway systems using advanced computational techniques. These approaches aim to capture the complex interactions between railway infrastructure and the surrounding environment, demonstrating that reliable models are essential for predicting stray-current behavior and for supporting the design of appropriate mitigation measures. Other studies adopt a more comprehensive perspective by considering the combined effects of rail voltage, track geometry, and environmental characteristics. Within this context, it has been shown that lumped-parameter circuit models—despite their apparent simplicity compared with distributed-parameter formulations—can still provide accurate results. This is mainly due to the low-frequency or quasi-DC nature of stray current phenomena, which does not require a highly refined spatial discretization along the track. Furthermore, several modeling approaches originally developed for DC metro systems have proven valuable for railway applications, given the strong similarities between the two contexts [8, 9].

Despite significant progress in recent years, stray-current mitigation remains an active research area. The increasing complexity of railway infrastructures and the continuous evolution of traction technologies highlight the need for further investigation and collaboration among researchers, infrastructure managers, and industry stakeholders [10–13].

An additional challenge emerging from the literature concerns the increasing topological complexity of circuit-based models used to represent stray-current phenomena. While the inclusion of numerous elements may improve the system's physical representation, it also introduces practical difficulties. Many components require extensive effort to determine their electrical parameters and increases the time needed to assemble and validate the model. Moreover, complex circuit structures increase the likelihood of modeling errors during implementation. These aspects can conflict with the operational constraints typical of industrial environments, such as those faced by railway infrastructure operators, who require calculation tools to support design activities and predictive maintenance within strict timeframes.

The present work originates from a collaborative research project involving the Italian railway infrastructure manager. The study focuses on the experimental validation of a multiconductor transmission line (MTL) model for estimating rail voltage and the associated stray current flowing into the surrounding soil and buried structures on operating railway lines. The objective is to assess whether this modeling technique can provide rail potential estimates comparable with measurements obtained along real railway tracks [14–17]. A more detailed critical analysis of the literature on the advantages and disadvantages of lumped, distributed, and hybrid circuit models is presented in [18], it is worth noting that lumped-parameter models often suffer from spatial discretization errors and high structural complexity in multiconductor scenarios, whereas purely distributed models can become mathematically intractable for complex, non-uniform topologies. The hybrid approach proposed here aims to balance rigorous analytical formalization with computational feasibility.

The proposed modeling framework is designed to be adaptable to different railway configurations: single rail tracks, multi-rail tracks, and railway tracks in the presence of buried conductive structures such as pipelines. The methodology adopted in this study builds on and extends the framework introduced in [18], which models the railway system as a lumped-parameter circuit. In that previous formulation, the fundamental building block of the model consists of an elementary lumped-parameter circuit cell with Π topology (Π-LP). Within this representation, the longitudinal (or 'horizontal') branch models the rail by means of a series combination of resistance and inductance, while the transversal (or 'vertical') branch accounts for the conductance between the rail and the surrounding earth. The proposed model consists of the hybridization of the Kirchhoff Laws describing the so-called 'aerial' part of the railway system, such as the traction power stations (TPS), the line of contact (LOC), and train with the telegraphers equations [19] in matrix form that describe the electrical behavior of the rails over the ground and the coupling with eventual buried conductors. The lumped-parameter approach used in [18] requires discretizing the circuit into multiple elementary cells (in our case, of Π type), which increases circuit complexity and may lead to accuracy issues. The distributed nature of the system considered by the telegrapher equations overcomes these limitations, introducing a continuous behavior of the electrical parameters and an inherent formulation of the multiconductor coupling case, as shown in one of the sections. Although not the focus of this work, this latest feature makes it easier to consider the electrical properties of complex multi-layer terrains. The formulation of the equations starts with the simple single-conductor case of a single-rail track without any coupled external structure and is extended to the case of a single-rail track with a buried conductor. The validation of the formulation and its numerical solution is achieved through a two-step approach. First, an algorithmic cross-validation is performed by comparing the computed results with a traditional commercial circuit simulator (LTSpice [20]). Since LTSpice relies on a modified nodal analysis algorithm, which is structurally different from the proposed Tableau analysis, a close agreement between them indicates that the mathematical implementation is structurally sound and free from algorithmic bugs. Second, the definitive physical validation of the model is provided by directly comparing the simulated curves against experimental field measurements. Following the experimental validation presented in this study, the model will serve as the basis for further developments within the project. Future extensions may incorporate more detailed soil representations and local rail insulation defects. For the actual railway systems considered in this work, the model's parameters have been determined using nominal or design values provided by the Italian railway operator (RFI) or measurements performed by the same operator. For the virtual one, the values have been estimated based on the relevant technical literature [21–23]. The novelty of this approach can be assessed in two major contributions: the first one concerning the use of a hybrid set of equations, combining both lumped and distributed circuit modeling; this proposed approach improves the accuracy of the modeling results with respect to the lumped-parameter Π-cell approach, by avoiding the discretization error introduced by a finite number of cells (as quantified in the appendix, table A1). Whereas the second one involves the modeling extension to a multiconductor case allowing to take into account, in the same analytical model, of multiple conductive parts relevant to a realistic railway infrastructure.

The paper's structure is as follows: section (2.1) presents the hybrid single-conductor transmission line equations for a virtual single-rail track without a parallel buried conductor. section (2.1) validates the approach by comparing the computed results with those obtained by the commercial circuit simulator. section (3.1) is devoted to extending the formulation of section 2.1 to a MTL problem. In this case, section (3.2) validates the results by comparing the computed values with those obtained from the circuit simulator. In this case, the limitations of the commercial software are highlighted. section (4). Applies the proposed circuit formulation to the real single-rail track from Francavilla Fontana to Brindisi (a railway line in a flat and dry region of the south of Italy), where some reliable measurements of the rail voltage [18] have been performed and are available. In this case, a virtual ground buried pipe has been imagined running parallel to the line, and the stray current induced on it has been computed and compared with those obtained by LTSpice. section (5). Draws some conclusions.

2. Circuit approach

Let us consider a section of a single-rail track of a railway system. The section is limited by the two traction power stations located at the left end (position x_{in}) and the right end (position x_{fin}). The length of the track is given by $\text{Len} = x_{\text{fin}} - x_{\text{in}}$.

The two TPS are electrically represented by their Thevenin equivalent. The left TPS is equivalent to the DC voltage source V_S in series with the equivalent resistance $R_{\text{Th-}S}$ (not shown in figure 1 because

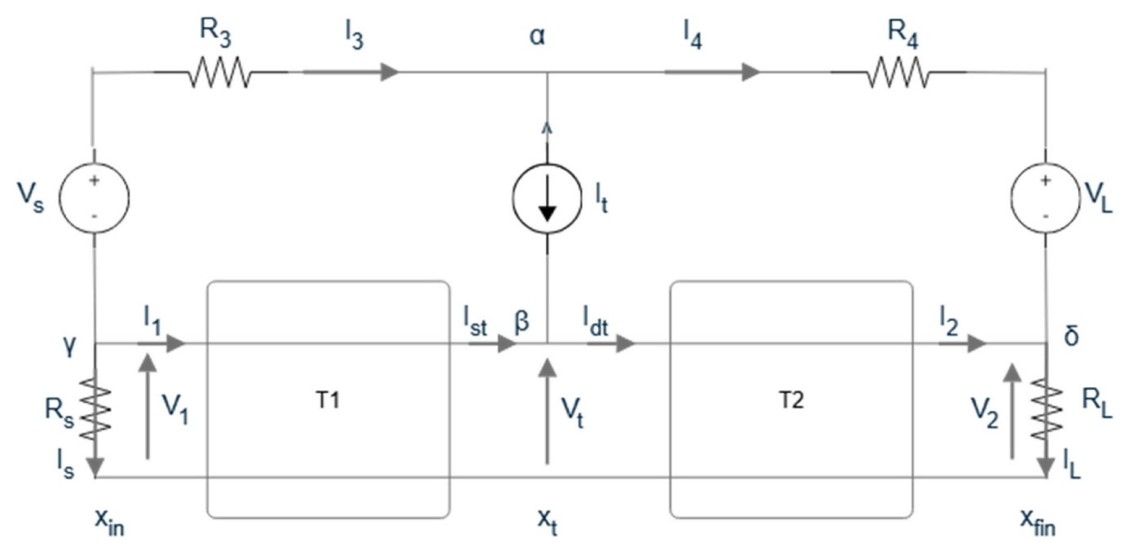

Figure 1. General schematic of the circuit model for the single-rail track configuration.

embedded in R_3). The right TPS is equivalent to the DC voltage source V_L in series with the equivalent resistance $R_{\text{Th-}L}$ (not shown in figure 1 because embedded in R_4).

The resistances of the overhead contact line or LOC from the TPSs to the train, represented by the DC current source I_t at position X_t, are R_{LOC} (X_t-X_{in}) and R_{LOC} (X_{fin}-X_t) in which R_{LOC} is the per unit length (p.u.l.) resistance of the LOC. These resistances are not shown in figure 1 but are also embedded in R_3 and R_4, as:

$$R_3 = R_{\text{Th}-\text{S}} + R_{\text{LOC}}\left(x_{\text{t}} - x_{\text{in}}\right) \tag{1a}$$

$$R_4 = R_{\text{Th}-\text{L}} + R_{\text{LOC}}\left(x_{\text{fin}} - x_{\text{t}}\right). \tag{1b}$$

The single-rail track is considered, with respect to the ground, as a pure resistive transmission line (rails' self and mutual inductances and capacitances are neglected).

R_S is the input impedance of the section of the track looking from x_{in} to the left. In the assumption that this section has no relevant discontinuities, its value is equal to its characteristic impedance

$$R_S = \sqrt{\frac{R_{\text{bin}-\text{S}}}{G_{\text{re}-\text{S}}}} \tag{2a}$$

where $R_{\text{bin-S}}$ is the per p.u.l. self-resistance of the rail, and $G_{\text{re-S}}$ is the p.u.l. earth conductance of this part of the rail.

Similarly, RL is the input impedance of the section of the track looking from x_{fin} to the right. With the same assumption above, it is defined as

$$R_{\text{L}} = \sqrt{\frac{R_{\text{bin}-\text{L}}}{G_{\text{re}-\text{L}}}}. \tag{2b}$$

For the single-rail track under consideration, between x_{in} and x_{fin} the p.u.l. self resistance of the rail is R_{bin} and the rail-to-earth p.u.l. conductance is G_{re}. Because of this the characteristic impedance of the rail section is

$$Z_{\text{c}} = \sqrt{\frac{R_{\text{bin}}}{G_{\text{re}}}} \tag{3a}$$

and the propagation constant m is

$$m = \sqrt{R_{\text{bin}} G_{\text{re}}} \tag{3b}$$

V_1, V_{t} and V_{L} are the rail voltages at the beginning x_{in}, at the train position X_{t} and at the end x_{fin} of the considered section.

The two sections of the track to the left and right of the train are described by two-port networks T1 and T2, with their inverse and direct transfer equations, respectively.

For the two-port network T_1 the inverse transfer equations in matrix form are

$$\begin{bmatrix} V_t \\ I_{\mathrm{st}} \end{bmatrix} = T_{1i} \begin{bmatrix} V_1 \\ I_1 \end{bmatrix} \tag{4a}$$

in which

$$T_{1i} = \begin{bmatrix} A_{1d} & B_{1d} \\ C_{1d} & D_{1d} \end{bmatrix}^{-1} \tag{4b}$$

is the direct Transmission or Chain matrix [19]. In (4b) the direct auxiliary constants are defined as

$$A_{1d} = \cosh\left(m \cdot x_{\mathrm{t}}\right) \tag{5a}$$

$$B_{1d} = Z_{\mathrm{c}} \sinh\left(m \cdot x_{\mathrm{t}}\right) \tag{5b}$$

$$C_{1d} = Y_{\mathrm{c}} \sinh\left(m \cdot x_{\mathrm{t}}\right) \tag{5c}$$

$$D_{1d} = \cosh\left(m \cdot x_{\mathrm{t}}\right). \tag{5d}$$

For the two-port network T_2 the direct transfer equations in matrix form are

$$\begin{bmatrix} V_{\mathrm{t}} \\ I_{\mathrm{dt}} \end{bmatrix} = T_{2d} \begin{bmatrix} V_2 \\ I_2 \end{bmatrix} \tag{6a}$$

in which

$$T_{2d} = \begin{bmatrix} A_{2d} & B_{2d} \\ C_{2d} & D_{2d} \end{bmatrix} \tag{6b}$$

is the inverse Transmission or Chain matrix [19]. In (6b) the direct auxiliary constants are defined as

$$A_{2d} = \cosh\left(m \cdot (\mathrm{Len} - x_t)\right) \tag{7a}$$

$$B_{2d} = Z_{\mathrm{c}} \sinh\left(m \cdot (\mathrm{Len} - x_{\mathrm{t}})\right) \tag{7b}$$

$$C_{2d} = Y_{\mathrm{c}} \sinh\left(m \cdot (\mathrm{Len} - x_{\mathrm{t}})\right) \tag{7c}$$

$$D_{2d} = \cosh\left(m \cdot (\mathrm{Len} - x_{\mathrm{t}})\right). \tag{7d}$$

The formulation of the set of equations that describes the electrical behavior of the circuit in figure 1 follows the logic of the 'tableau' method [24]. The set of equations is built up by N_V independent Kirchhoff voltage law (KVL) equations, N_{I} independent Kirchhoff current law (KCL) and the two matrix equations (4) and (6).

The analysis of the graph and tree of the circuit in figure 1 gives $N_V = 3$ KVL equations

$$V_1 + V_{\mathrm{S}} - R_3 I_3 - R_4 I_4 - V_{\mathrm{L}} - V_2 = 0 \tag{8a}$$

$$V_1 - R_S I_{\mathrm{S}} = 0 \tag{8b}$$

$$V_2 - R_{\mathrm{L}} I_{\mathrm{L}} = 0. \tag{8c}$$

For the $N_I = 4$ independent nodes a, b, g and d, the KCL equations are

$$\mathrm{node}\alpha: \; I_3 - I_t - I_4 = 0 \tag{9a}$$

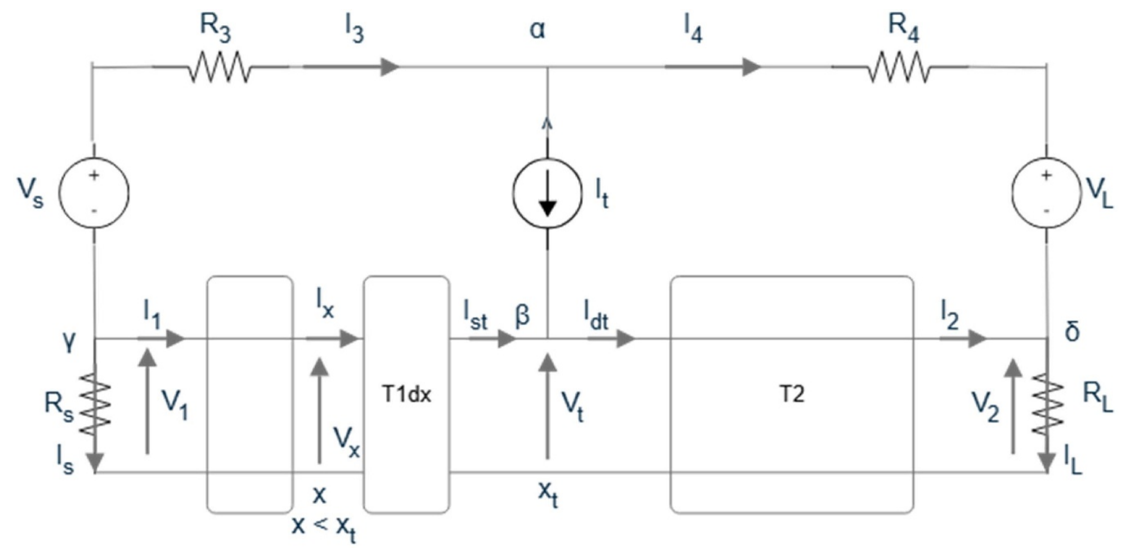

Figure 2. Schematic of the circuit model in figure 1 after splitting T_1 in 2 two-port networks.

$$\mathrm{node}\beta: \; I_{st} + I_t - I_{dt} = 0 \tag{9b}$$

$$\mathrm{node}\gamma: -I_3 - I_S - I_1 = 0 \tag{9c}$$

$$\mathrm{node}\delta: \; I_2 + I_4 - I_L = 0. \tag{9d}$$

Finally, at equations (8) and (9), one should add (4a) and (6a) in order to have the full set of equations that can be expressed in matrix form as

$$\mathrm{TB} \cdot U = S \tag{10}$$

where TB is the 11 × 11 matrix Tableau of the coefficients [24], U is the 11 × 1 column vector of the unknowns, and S is the 11 × 1 column vector of the source (or known) terms. The solution of (10)

$$U = \mathrm{TB}^{-1} \cdot S \tag{11}$$

gives the column vector $U = [V_1 \; V_2 \; V_\mathrm{t} \; I_1 \; I_2 \; I_3 \; I_4 \; I_\mathrm{S} \; I_\mathrm{L} \; I_\mathrm{st} \; I_\mathrm{dt}]$ evaluated when the train is at X_t along the track and absorbing the traction current I_t.

To compute the rail voltage at a generic position x along the section, it is convenient to introduce two other two-port networks as shown in figure 2. Let us consider the case when the generic location x is less than the position X_t of the train ($X < X_\mathrm{t}$). Since one knows, from (11), the values of V_t and $I_\mathrm{st,}$ the direct transfer equation (12) can be used to evaluate the rail voltage V_x and the associated current I_x at the generic position x.

$$\begin{bmatrix} V_x \\ I_x \end{bmatrix} = T_{1dx} \begin{bmatrix} V_t \\ I_{st} \end{bmatrix} \tag{12}$$

where

$$T_{1dx} = \begin{bmatrix} A_{1dx} & B_{1dx} \\ C_{1dx} & D_{1dx} \end{bmatrix} \tag{13}$$

and

$$A_{1dx} = \cosh\left(m \cdot (x_\mathrm{t} - x)\right) \tag{14a}$$

$$B_{1dx} = Z_c \sinh\left(m \cdot (x_t - x)\right) \tag{14b}$$

Table 1. Source (or active) circuit parameters.

V_S	V_L	I_t
3000 V	3000 V	1200 A

Table 2. Passive circuit parameters.

$R_{Th\text{-}S}$	$R_{Th\text{-}L}$	R_S	R_L	R_{LOC}	R_{bin}	G_{re}
0.15 W	0.15 W	0.0424 W	0.0941 W	0.05725 W km^{-1}	0.015 W km^{-1}	0.5 S km^{-1}

$$C_{1dx} = Y_c \sinh\left(m \cdot (x_t - x)\right) \tag{14c}$$

$$D_{1dx} = \cosh\left(m \cdot (x_t - x)\right). \tag{14d}$$

If the generic position x is greater than X_t ($X > X_t$), then the same procedure is applied by splitting the two-port network T2. In this case one has

$$\begin{bmatrix} V_x \\ I_x \end{bmatrix} = T_{2ix} \begin{bmatrix} V_t \\ I_{dt} \end{bmatrix} \tag{15}$$

where

$$T_{2ix} = {T_{2dx}}^{-1} = \begin{bmatrix} A_{2dx} & B_{2dx} \\ C_{2dx} & D_{2dx} \end{bmatrix}^{-1} \tag{16}$$

and

$$A_{2dx} = \cosh\left(m \cdot (x - x_t)\right) \tag{17a}$$

$$B_{2dx} = Z_c \sinh\left(m \cdot (x - x_t)\right) \tag{17b}$$

$$C_{2dx} = Y_c \sinh\left(m \cdot (x - x_t)\right) \tag{17c}$$

$$D_{2dx} = \cosh\left(m \cdot (x - x_t)\right). \tag{17d}$$

2.1 Validation

In order to validate the proposed circuit solution, its results are compared with those obtained by LTSpice, a commercial circuit simulator. A single-rail track of length Len = 30 km is considered with two TPS at the ends. Tables 1 and 2 summarize the main parameters of the circuit model whose values are equal to or very close to actual ones.

The train moves from left to right (from x_{in} to x_{fin}) absorbing a traction current of $I_t = 1200$ A. This constant value has been used solely to make the results and comparison more understandable; nothing in the proposed circuit solution requires a spatially constant traction current.

Figure 3 shows the comparison of the values of the voltage rail V_r computed at the location of the train ($V_r\ (X_t) = V_t$) by the proposed circuit solution and LTSpice. V_r is computed at 7 different values of X_t: 0, 5, 10, 15, 20, 25 and 30 kilometers respectively. It is worth noting that using LTSpice (or any other commercial circuit simulator) requires 7 separate runs, each with the circuit topology adjusted according to the train's position. In the proposed procedure, the same results are obtained in a single run. The agreement between the two sets of values is very good.

Figure 4 reports the spatial distribution of the rail voltage V_r along the entire line when the train is at $x_t = 5$, 10, 15 and 20 km, respectively (the position of the train is given by the vertex of the inverted-V shape of the spatial distribution of V_r). The continuous lines represent the values computed by the proposed method, the asterisks those computed by LTSpice. Again, the agreement is excellent. As already mentioned, each of the four sets of LTSpice results requires a separate simulation with a change of topology in the schematics and/or netlist.

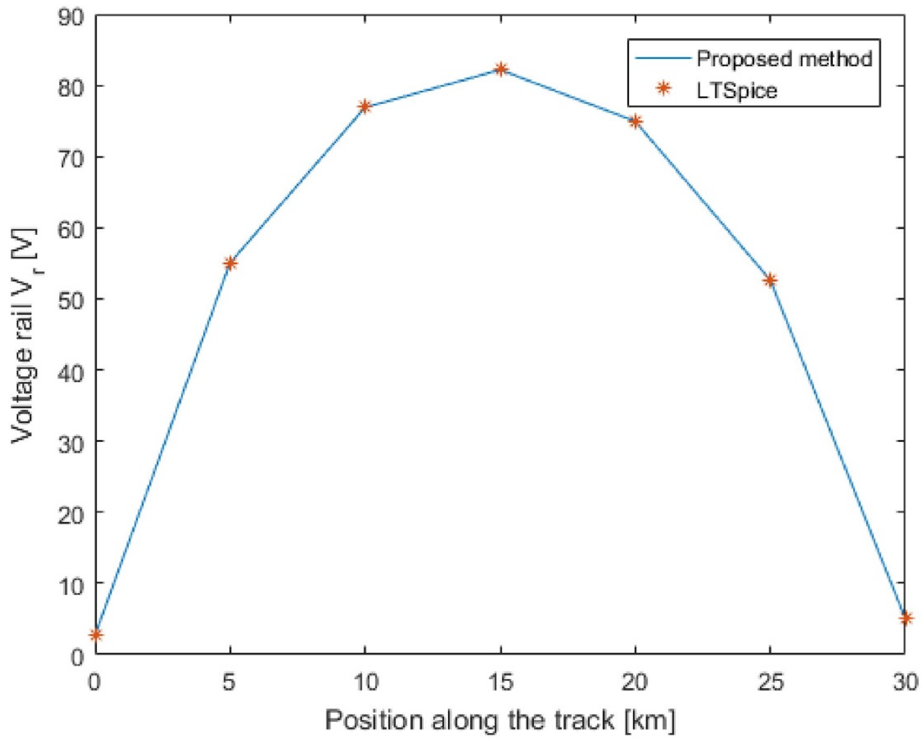

Figure 3. Spatial distribution of the rail voltage V_r at the same position of the train $V_r(x_t) = V_t$ for seven different locations of the train along the track proposed method (—) and LTSpice (*).

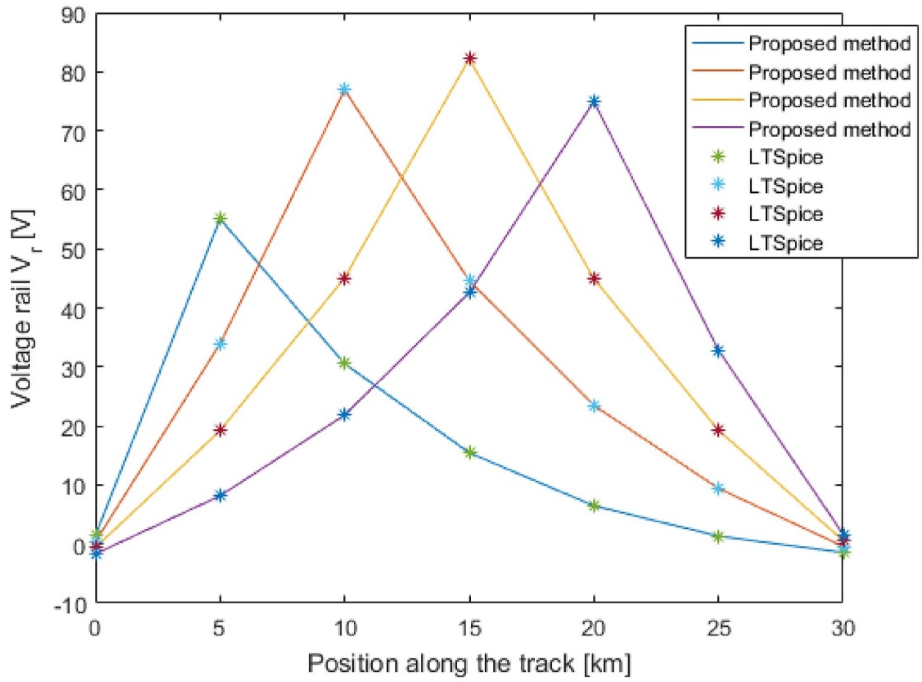

Figure 4. Spatial distribution of the rail voltage V_r along the track when the train is at four different locations of the train along the track: proposed method (—) and LTSpice (*).

In terms of computational efficiency, the proposed method and the LTSpice solution have comparable run times for each single run. It should be mentioned that the developed software for the formation of the set of equation (10) and its solution in (11) have not been optimized from a computational point of view. However, it should be emphasized that while the LTSpice lumped model requires the solution of a massive nodal matrix (N = 150 cells), the proposed approach solves a compact hybrid formulation

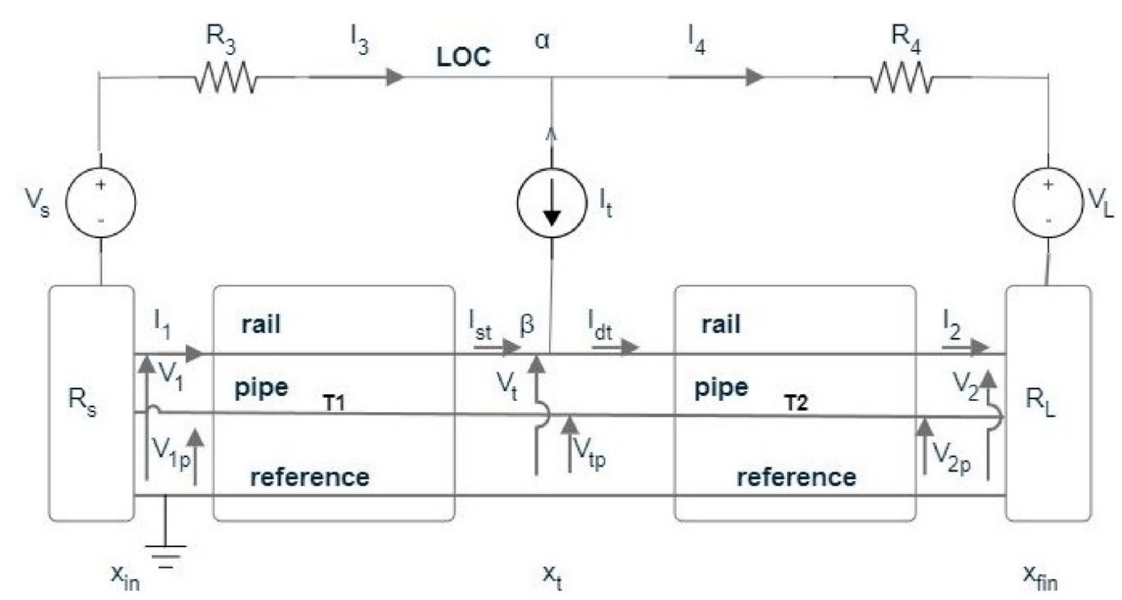

Figure 5. General circuit representation of the view of the rail-pipe configuration.

analytical in nature. Optimization of the dedicated solution code represents a clear target for future work to fully exploit this structural advantage across complex multi-layer terrains.

3. Extension to multiple conductors

The proposed approach for forming the set of equations describing the single-rail track case can be extended to multiple conductors, such as a two-rail track or a single-rail track with a ground-embedded metallic pipe. We have considered this latter case, which is relevant to predictive anti-corrosion maintenance of ground-embedded structures in the presence of induced stray currents.

Figure 5 shows a general view of the rail-pipe configuration. Above the earth, the two TPS, the LOC and the equivalent current source I_t representing the train are unchanged with respect the single-track case. At the earth level a 2 + 1 multiconductor line is considered: the two 'active' conductors are the single-rail and the ground embedded pipe. Their voltages are referred to a third virtual reference conductor that complete the multiconductor system.

At the left and right ends of the line, two termination networks are represented by the diagonal matrices $\mathbf{R}_s$ and $\mathbf{R}_L$ (in this case matrices are in bold) whose elements are the terminations impedances of the rail track and the pipe at the left and right ends, respectively. They are defined as

$$\boldsymbol{R}_S = \begin{bmatrix} R_S & 0 \\ 0 & R_{Sp} \end{bmatrix} \tag{18a}$$

$$\boldsymbol{R}_L = \begin{bmatrix} R_L & 0 \\ 0 & R_{Lp} \end{bmatrix} \tag{18b}$$

where the rail parameters R_s and R_L have been introduced in (2a) and (2b), and the pipe parameters R_{sp} and R_{Lp} are set to $R_{sp} = R_{Lp} = \infty$, that is to say the pipe is considered electrically isolated at both ends.

The coupling between the rail and the ground embedded pipe is given through the direct and inverse transfer matrices associated to the multi-ports networks T1 and T2. In this case, the transfer matrices are matrix-of-matrices, that is, their elements A, B, C, and D are, in turn, matrices.

To build these matrices one resorts to the modal analysis [19]. The first step is to build the matrices of the p.u.l. parameters of rail and pipe. The p.u.l. matrix for the longitudinal resistances is

$$R = \begin{bmatrix} R_{\text{bin}} & 0 \\ 0 & R_{\text{pipe}} \end{bmatrix}. \tag{19a}$$

In which R_{bin} is the p.u.l. resistance of the rail and R_{pipe} is the equivalent p.u.l. of the pipe.

$$G = \begin{bmatrix} G_{re} & G_{rp} \\ G_{rp} & G_{pe} \end{bmatrix} \tag{19b}$$

where G_{re} and G_{pe} are the p.u.l. self conductances of rail and pipe and G_{rp} is the mutual conductance between them. Let us define the product matrices $RG = R \cdot G = GR$ and extract their eigenvectors $\boldsymbol{T}$ and eigenvalues $\boldsymbol{\gamma}$. The matrix $\boldsymbol{\gamma}$ is diagonal. From $\boldsymbol{\gamma}$ one can obtain the diagonal matrix $\mathbf{m}$ of the modal propagation constants

$$m = \begin{bmatrix} m_1 & 0 \\ 0 & m_2 \end{bmatrix} = \begin{bmatrix} \sqrt{\gamma}_1 & 0 \\ 0 & \sqrt{\gamma}_2 \end{bmatrix}. \tag{20}$$

From (20), one can compute the full matrix of the characteristic impedance of the two-conductor line, considering the coupling between them. The matrix $\mathbf{Z_c}$ (and its inverse $\mathbf{Y}_{\text{c}}$) is given by [19]

$$Z_{\text{c}} = T \cdot m^{-1} \cdot T^{-1} \cdot R \tag{21a}$$

$$Y_{\text{c}} = Z_{\text{c}}^{-1}. \tag{21b}$$

With all these elements one can define the matrices T_{1dx} and T_{2ix}. The first step is to evaluate the diagonal matrices

$$\text{COS}Hmx = \begin{bmatrix} \cosh(m_1\ell) & 0 \\ 0 & \cosh(m_2\ell) \end{bmatrix} \tag{22a}$$

$$\text{SIN}Hmx = \begin{bmatrix} \sinh(m_1\ell) & 0 \\ 0 & \sinh(m_2\ell) \end{bmatrix}. \tag{22b}$$

By using (20)–(22) the elements of the direct transfer matrix

$$T_{1d} = \begin{bmatrix} A_{1d} & B_{1d} \\ C_{1d} & D_{1d} \end{bmatrix} \tag{23}$$

are

$$A_{1d} = T \cdot \text{COS}Hmx \cdot T^{-1} \tag{24a}$$

$$B_{1d} = T \cdot SINHmx \cdot m^{-1} \cdot T^{-1} \cdot R \tag{24b}$$

$$C_{1d} = G \cdot T \cdot m^{-1} \cdot SINHmx \cdot T^{-1} \tag{24c}$$

$$D_{1d} = T \cdot COSHmx \cdot T^{-1}. \tag{24d}$$

The elements of the inverse transfer matrix

$$T_{2i} = \begin{bmatrix} A_{2i} & B_{2i} \\ C_{2i} & D_{2i} \end{bmatrix} \tag{25}$$

are

$$A_{2i} = A_{1d} \tag{26a}$$

$$B_{2i} = -T \cdot SINHmx \cdot m^{-1} \cdot T^{-1} \cdot R \tag{26b}$$

$$C_{2i} = -G \cdot T \cdot m^{-1} \cdot SINHmx \cdot T^{-1} \tag{26c}$$

$$D_{2i} = D_{1d}. \tag{26d}$$

In which the positions of (26a) and (26b) are due to the properties of the Transmission or Chain matrices [19]. The complete circuit in the presence of a multiconductor system network leads to a set of equations like that in (10), whose formal solution is the same as that in (11).

Table 3. Passive circuit parameters of the pipe.

R_{Sp}	R_{Lp}	R_{pipe}	G_{pe}	G_{rp}
100 MW	100 MW	0.0267 W	0.5 S km^{-1}	0.0015 S km^{-1}

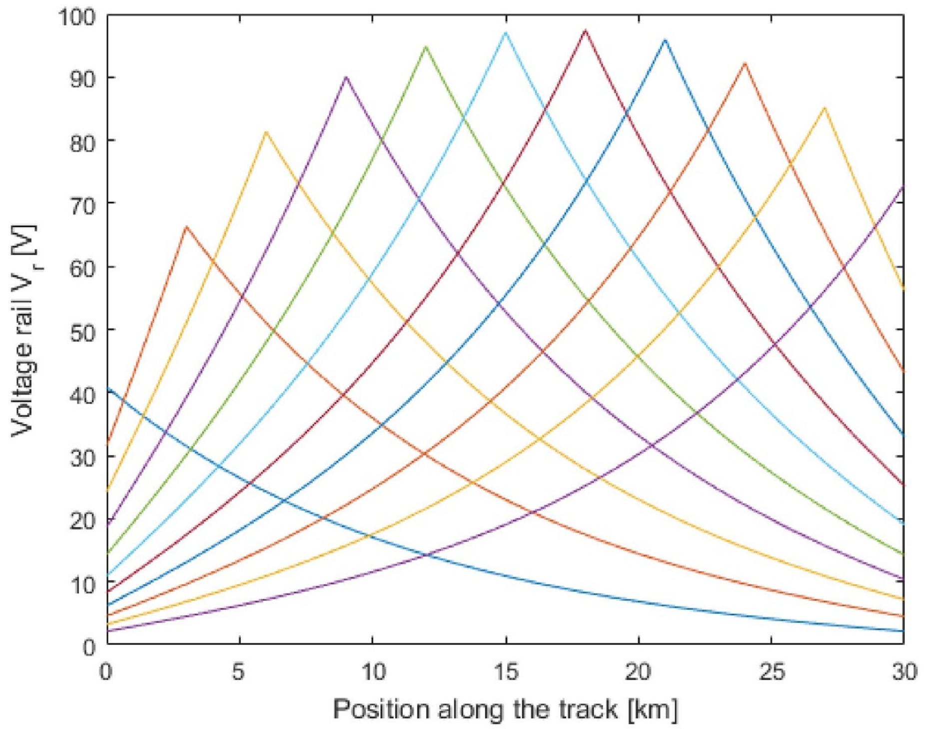

Figure 6. Spatial distribution of the rail voltage V_r along the track when the train is at eleven different locations along the track.

3.1 Validation

As in the validation of the proposed solution is performed by comparing the computed results with those obtained with LTSpice. The same single-rail track of length Len = 30 km is considered with two TPS at the ends. In parallel to the track a ground-embedded metallic pipe of the same length is placed at 20 m from the track. Tables 1 and 2 summarize the main parameters of the single-rail track circuit model.

Also, in this case, the train moves from left to right (from x_{in} to x_{fin}) absorbing a traction current of $I_t = 1200$ A. This constant value has been used solely to make the results and comparison more understandable; nothing in the proposed circuit solution requires a spatially constant traction current. The multiconductor nature of the circuit requires to give values to the other entries of the matrices (18) and (19). Table 3 reports the missing values:

Due to the nature of the matrices T in (23) and (25), the coupling between the rail and the pipe through the soil's conductance is analytically and completely accounted for in the distributed circuit formulation. It should be mentioned that LTSpice does not have in its libraries any analytical model for a coupled multiconductor line. Because of this, a discretized model of a cascade of resistively coupled P lumped-element cells has been used. After a systematic analysis of convergence (see appendix), the optimal number of cells was found to be $N = 150$. Over this number, the accuracy remains constant.

Figure 6 shows the spatial distribution of the values of the voltage rail V_r computed by the proposed circuit solution for 11 locations X_t of the train ($V_r\ (X_t) = V_t$): $X_t = 0$, 3, 6, 9, 12, 15, 18, 21, 24, 27 and 30 kilometers respectively. As previously mentioned, using LTSpice or any commercial circuit simulator requires 11 separate runs, each with the circuit topology adjusted according to the train's position.

Figure 7 reports the comparison between the values of the induced stray current I_p along the ground-embedded pipe, for different positions of the train along the single-rail track, computed by the proposed method (continuous lines) and by the cascaded lumped cells in LTSpice (asterisks). The agreement is good, though not perfect, due to the inherent approximation introduced by the lumped cells. At the ends of the pipe, the currents go to very small values due to the open circuit conditions set by the

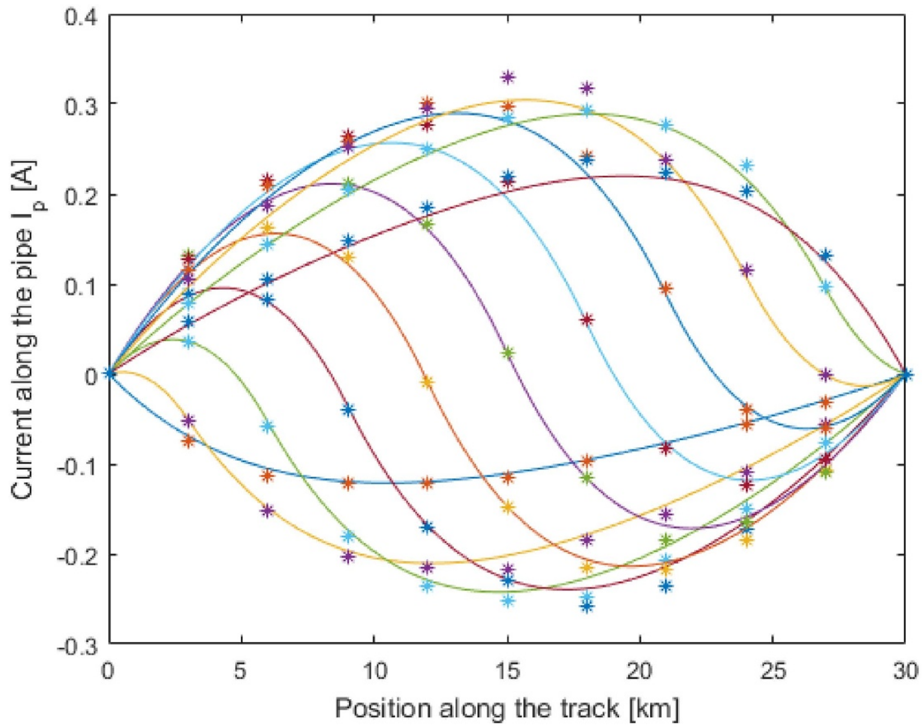

Figure 7. Spatial distribution of the induced stray currents I_p along the ground-embedded pipe when the train is at eleven different locations along the track, proposed method (—) and LTSpice (*).

Table 4. Nominal electrical parameters of the Francavilla Fontana–Brindisi railway line.

V_S			V_L		
3000 V			3000 V		
$\mathbf{R}_{\text{Th-}S}$	$\mathbf{R}_{\text{Th-}L}$	$\mathbf{R}_L$	$\mathbf{R}_{\text{LOC}}$	$\mathbf{R}_{\text{bin}}$	$\mathbf{G}_{\text{re}}$
0.15 W	0.15 W	0.0941 W	0.05725 W km^{-1}	0.015 W km^{-1}	0.13 S km^{-1}
$\mathbf{R}_{\text{Sp}} = \mathbf{R}_{\text{Lp}}$	$\mathbf{G}_{\text{pe}}$	$\mathbf{G}_{\text{rp}}$			
100 MW	0.13 S km^{-1}	0.0015 S km^{-1}			

equivalent resistances R_{Sp} and R_{Lp} in table 3. As already mentioned, the solution of the equations has also not been optimized to shorten running times. As a result, at the actual stage of software development, the computational efficiency of both approaches is equivalent.

3.2 Assessment of rail voltage and stray current phenomena in the Francavilla Fontana–Brindisi railway section

This section addresses the modeling of the railway line Francavilla Fontana–Brindisi. The investigation was initiated following reports of stray-current interference phenomena affecting a nearby gas pipeline. In collaboration with the RFI a measurement campaign was carried out to experimentally characterize the rail voltage of the traction system under normal operating conditions. The measurement procedures and results have been reported in [18] and not repeated here for the sake of brevity. For this line, the exact geological structure of the soil was not known. Only the general composition of the ground along the railway lines was available. The information on soil structure was inferred from measurements of rail-to-earth conductance (Gre). Based on this parameter and the available data, a first-order approximation was adopted by assuming that stray currents propagate through a homogeneous soil layer. This assumption comes from the specific location of the experimental validation, since it is performed on the Francavilla Fontana–Brindisi line running through a flat and dry region of southern Italy; therefore the assumption of a laterally uniform soil is geologically reasonable as a first-order approximation. In [18] a lumped circuit model has been used to evaluate the rail voltage without considering the presence of buried pipelines. In the following, the above developed multiconductor approach will be used either to compute the rail voltage along the line, to compare its values with those measured, and the stray currents flowing along a virtual buried pipeline. In this latter case, such values have not been measured;

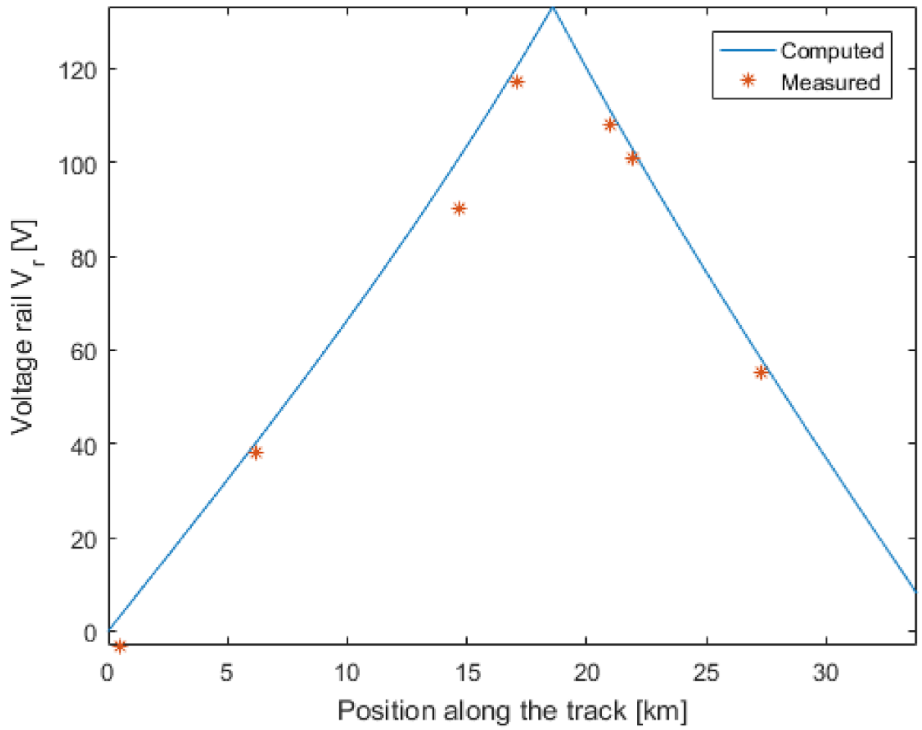

Figure 8. Spatial distribution of the induced voltage rail along the track when the train is at 18.5 km and it is absorbing $I_t = 1217$ A: proposed method (—) and measured (*).

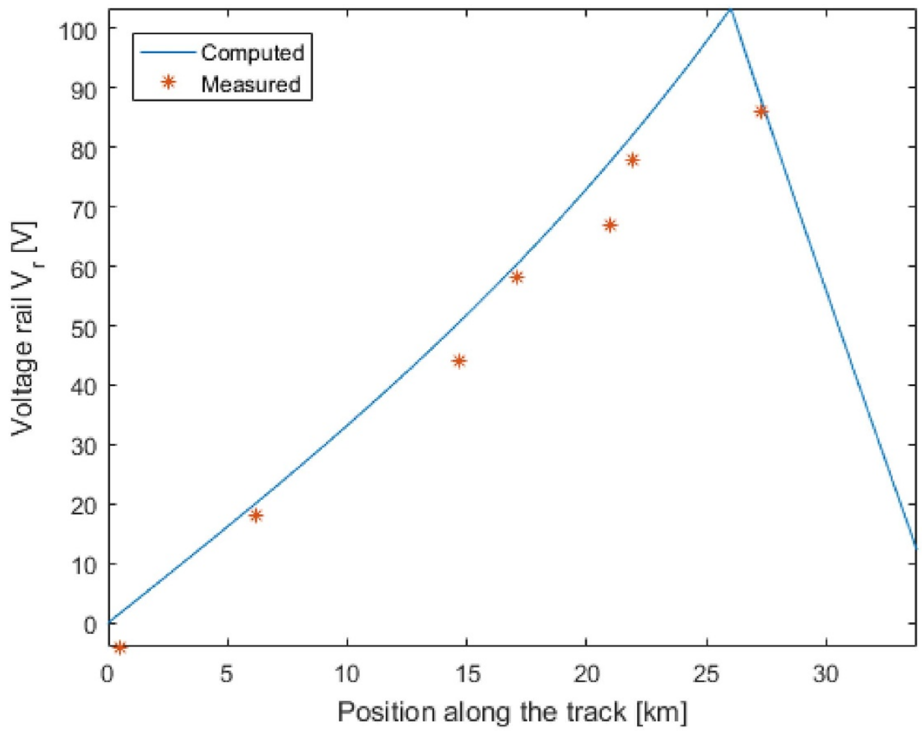

Figure 9. Spatial distribution of the induced voltage rail along the track when the train is at 26 km, and it is absorbing $I_t = 1190$ A: proposed method (—) and measured (*).

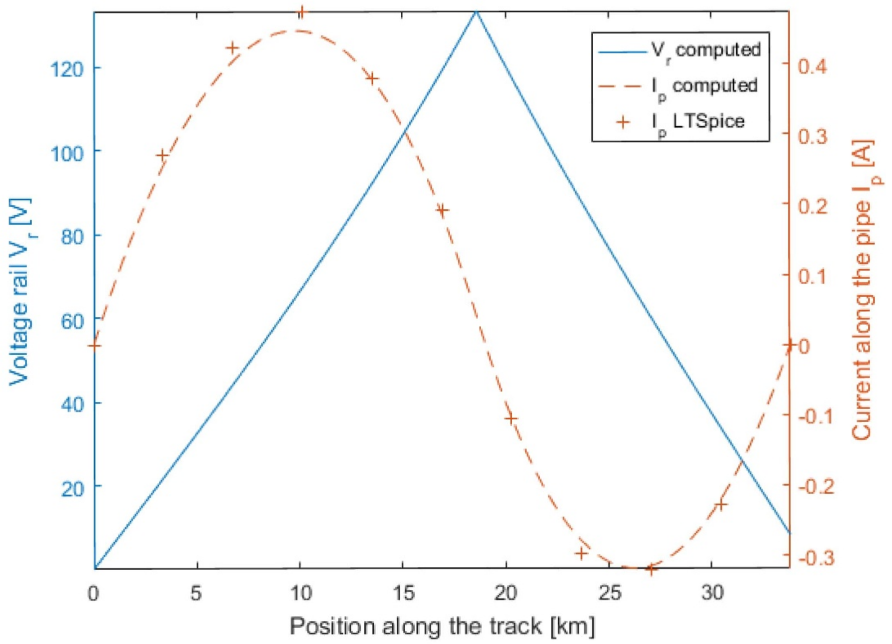

a

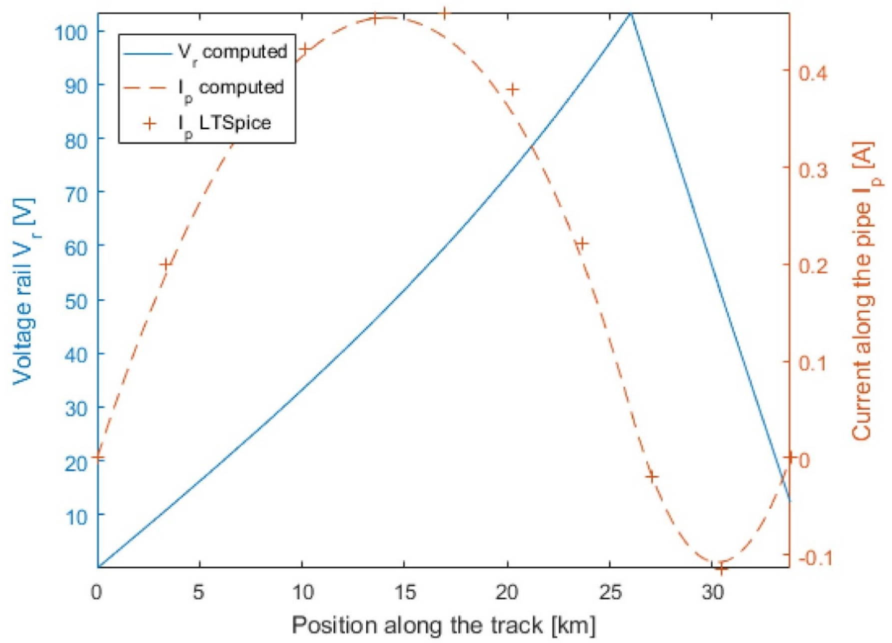

b

Figure 10. (a) Spatial distribution of the induced voltage rail V_r along the track and the current Ip along the virtual buried pipeline when the train is at 18.5 km and it is absorbing $I_t = 1217$ A: proposed method (continuous and dashed lines) and from LTSpice (+). (b) Spatial distribution of the induced voltage rail V_r along the track and the current Ip along the virtual buried pipeline when the train is at 26 km and it is absorbing $I_t = 1190$ A: proposed method (continuous and dashed lines) and from LTSpice (+).

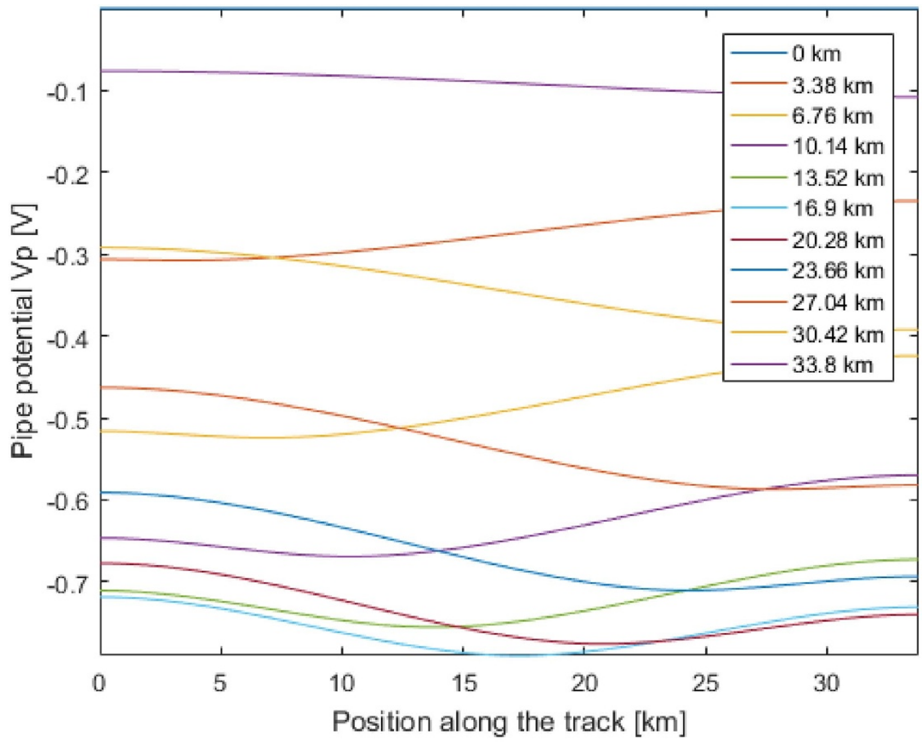

Figure 11. Spatial distribution of the computed induced potential V_p on the virtual ground buried pipeline when the train is at 11 different locations along the track.

they are computed by the proposed approach and validated by other values independently computed by the already mentioned commercial circuit simulator.

The railway line connecting Francavilla Fontana to Brindisi is subdivided into several operational sections—namely Francavilla Fontana–Oria, Oria–Latiano, Latiano–Mesagne, and Mesagne–Brindisi—covering a total length of 33.8 km. The relevant electrical parameters for the used MTL model are summarized in table 4: they were derived partly from the nominal specifications of the electrical infrastructure parameters and partly from the experimental measurements reported in [18]. The parameters associated with the virtual pipeline were estimated by also considering the relevant technical literature [21–23].

Figures 8 and 9 report the comparison between computed and measured values of the voltage rail Vr when the train is at 18.5 km and 26 km from the Francavilla Fontana station (located at the origin $x = 0$ km of the abscissa), and it is absorbing the measured current $I_t = 1217$ A and $I_t = 1190$ A, respectively.

The agreement between computed and measured results has been quantified using the root-mean-square error (RMSE) between the two sets. For the data in figure 8 RMSE figure 7 = 3.37 V for those in figure 9 it is RMSE figure 8 = 4.31 V.

There is a correlation between the spatial distribution of the rail voltage V_r and the stray currents flowing on the buried pipeline. figures 10(a) and (b) show, on the same graph, Vr (left vertical axis) and the current I_p through the pipeline (right vertical axis) for the train at 18.5 km (It = 1217 A) and 26 km ($I_t = 1190$ A), respectively. I_p has also been computed in LTSpice using an approximate lumped-circuit model, as described in section IIIb. It is worth noting that the current I_p is null at the termination of the pipe due to the open-circuit conditions and inverts its polarity in correspondence with the maximum value of the voltage rail that is always located at the train position [18].

The impact of the rail voltage on the induced potentials along the virtual ground buried pipeline is shown in figure 11. For 11 different locations of the train along the track, as reported in the figure inset, there are 11 spatial distributions of V_p.

The next figures 12(a) and (b) reports on the same graph the spatial distribution of the induced pipe voltage V_p (continuous line, left vertical axis) and the spatial distribution of the induced stray-current I_p (dashed line, right vertical axis) along the virtual buried pipeline when the train is moving along the Francavilla Fontana–Brindisi line and it is located at 18.5 km and 26 km, respectively. The inversion of

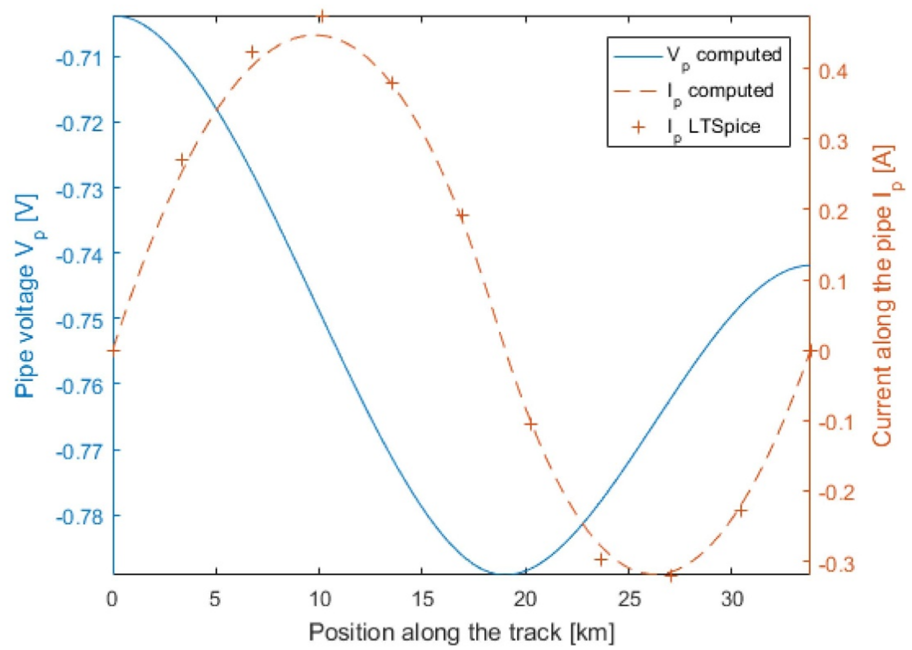

a

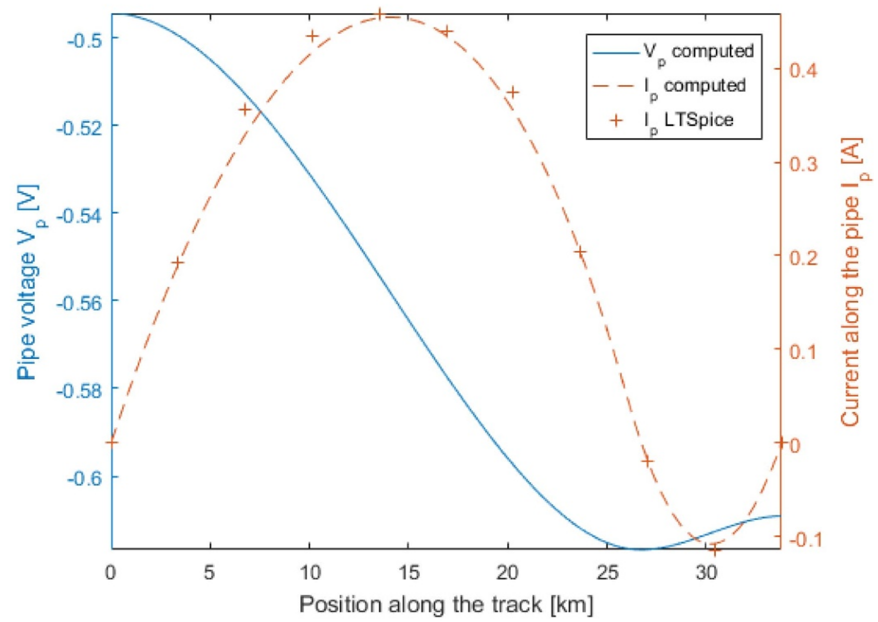

b

Figure 12. (a) Spatial distribution of the computed induced potential V_p and current I_p along the virtual ground buried pipeline when the train is at 18.5 km and it is absorbing $I_t = 1217$ A: proposed method (continuous and dashed lines) and from LTSpice (+). (b) Spatial distribution of the computed induced potential V_p and current I_p along the virtual ground buried pipeline when the train is at 26 km and it is absorbing $I_t = 1190$ A: proposed method (continuous and dashed lines) and from LTSpice (+).

the polarity of the stray current I_p induced on the ground buried structure is strictly related to the position of the train along the railway line on the surface. As previously done, the computed results of I_p by the proposed MTL method are compared with those obtained by a cascade lumped circuit model solved in LTSpice, whose results are shown as crosses ('+') in the two figures. The visual agreement is acceptable.

4. Conclusions

This work has demonstrated that a MTL model can effectively be employed to estimate rail voltages and the associated stray currents in electrified railway systems. Determining both the magnitude of stray currents and their distribution along a ground buried pipeline is particularly valuable for the predictive assessment of stray-current-induced corrosion in nearby infrastructures.

One of the main advantages of this MTL representation is its ability to achieve an acceptable level of accuracy for practical engineering applications while substantially limiting modeling effort and computational complexity. This balance allows engineers and operators to perform rapid analyses and make informed decisions without the need to address the full physical complexity of the system. Such a feature is especially important in operational and industrial environments, where the priority is often the availability of reliable and quickly interpretable results rather than highly detailed theoretical models.

By focusing on the most relevant electrical interactions within the traction return circuit and the nearby structures, multiconductor models simplify the analysis workflow and enable faster evaluations of system performance, troubleshooting, and preliminary design. In addition, their relative ease of implementation makes them accessible to a broader group of users, which is particularly advantageous in contexts where simplicity, speed, and robustness are essential. Consequently, the multiconductor lines modeling approach is a practical engineering tool that supports efficient decision-making without significantly compromising the reliability of the analysis.

The good agreement obtained between the simulated results and the experimental measurements confirms that the main physical mechanisms governing the system behavior are adequately captured by the proposed approach. This is particularly true for railway sections characterized by relatively uniform conditions along the track, such as open-air segments without tunnels or viaducts. Under these circumstances, the model allows the extraction of meaningful information on rail voltage levels and stray-current distributions around buried metallic ground structures, which are relevant for both design and safety evaluations.

Although more detailed circuit representations could further improve the accuracy of stray current predictions, estimating their order of magnitude already provides useful guidance during the early stages of railway system design. In particular, these estimates can assist engineers in assessing the appropriate spatial arrangement between railway tracks and nearby infrastructures that may be sensitive to stray currents, including buried pipelines, industrial grounding systems, and components of adjacent power networks.

A more refined characterization of stray current propagation may be necessary in more complex environments, such as tunnels, where layered structures—typically reinforced concrete and insulating materials—can significantly alter the electrical conductance of the current return path. Future research will therefore focus on extending the MTL modeling framework to represent heterogeneous scenarios using a more general circuit formulation.

To support this development, additional investigations will include field measurements performed at multiple locations along the railway line to evaluate possible spatial variations in the rail-to-earth conductance (G). These measurements will be complemented by a detailed assessment of the local underground and geological conditions. Such information is expected to be increasingly accessible thanks to the detailed documentation available for modern railway construction and installation projects.

Building on the encouraging results obtained in this study, future work will also address railway configurations that include both tunnels and viaducts. In these situations, assuming a uniform rail-to-earth conductance along the track is no longer adequate, and the modeling approach must incorporate spatially varying electrical parameters to accurately represent the system's behavior in terrains with complex vertical and longitudinal composition.

In such scenarios, assuming a uniform rail-to-earth conductance along the track is no longer adequate. To overcome this limitation, future developments will incorporate longitudinal variations of soil properties by adopting a piecewise-homogeneous segmentation approach, solving the global boundary value system through the sequential cascading of local multiconductor transmission matrices.

Data availability statement

The data cannot be made publicly available upon publication due to legal restrictions preventing unrestricted public distribution. The data that support the findings of this study are available upon reasonable request from the authors.

Author contributions

Lino Di Leonardo 0000-0001-8041-1528
Data curation (equal), Methodology (equal), Software (equal), Visualization (equal), Writing – original draft (equal)

Francesco de Paulis 0000-0002-5613-2454
Data curation (equal), Validation (equal), Visualization (equal), Writing – review & editing (equal)

Antonio Orlandi 0000-0001-5301-2820
Conceptualization (equal), Methodology (equal), Software (equal), Writing – original draft (equal)

Fabio Sbarra
Data curation (equal), Project administration (equal), Validation (equal), Writing – review & editing (equal), Supervision (equal)

Marco Camomilla
Conceptualization (equal), Supervision (equal), Writing – review & editing (equal), Project administration (equal)

Appendix

Let us consider a pure resistive transmission line with the same geometrical (length of 30 km) and electrical (per unit length rail resistance and ground conductance) parameters of the single-rail track in section 3.2. The line is modeled as a cascade of progressively increasing numbers of lumped P cells: first only one, then two, up to a number of cells for which the chosen figure of merit stably converges to its value obtained by the exact solution of a distributed transmission line model (equivalent to an infinite number of P cells). The significant figure of merit chosen is the transfer function *F* between the voltage V_L at the end of the line, across the termination impedance Z_L when Z_L is equal to the characteristic impedance Z_c, and the voltage V_1 at the beginning of the line

$$\Phi = \frac{V_L}{V_1}\Big|_{Z_L=Z_c}. \tag{A1}$$

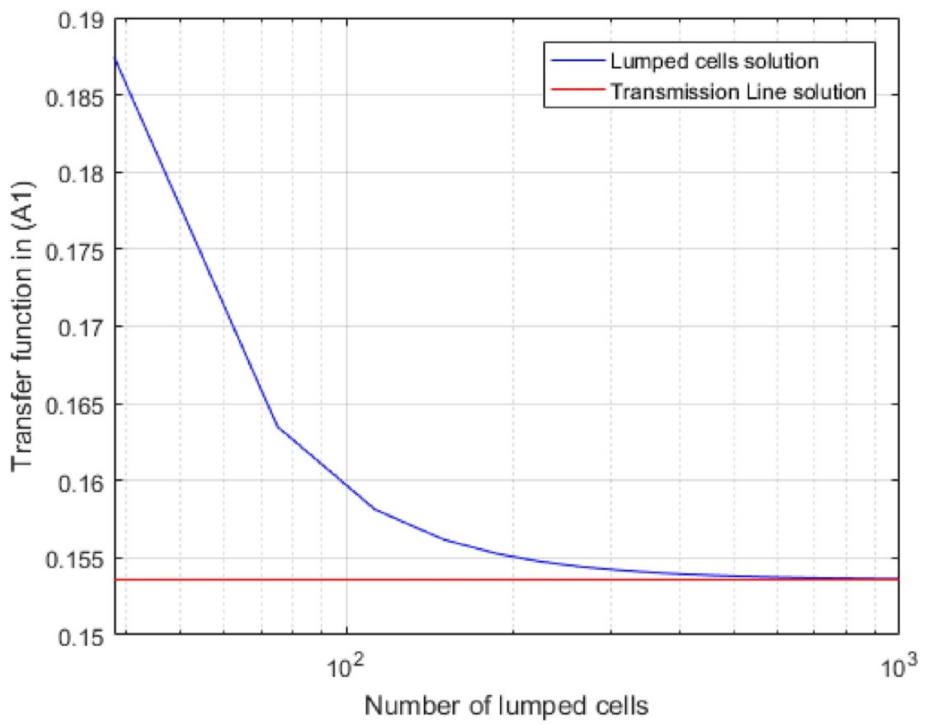

Figure A1. Convergence analysis of *F* in (A1).

Figure A1 shows that as the number of P lumped cells increases, F it tends to the value of the theoretical transmission line solution.

As an example, table A1 extracts from figure A1 a few values of the percentage error between the solution by using lumped P cells and the solution by using a distributed transmission line model with respect to the number of cells. A number between 110 and 180 cells gives an acceptable approximation, so limiting the number of used cells in favor of the computing performance.

Table A1. Percentage error between lumped cells and transmission line solution.

Number of $\prod$ cells	75	110	180	900
Error %	6.45	2.96	1.08	0.05

References

[1] Siranec M, Regula M, Otcenasova A and Altus J 2020 *Measurement and Evaluation of the Stray Currents from the DC Electric Traction Systems* (ELEKTRO) pp 1–6

[2] Regula M, Siranec M, Otcenasova A and Hoger M 2022 Possibilities of the stray current measurement and corrosive risk evaluation *Electr. Eng.* **104** 2497–513

[3] Wieczorek G, Bernacki K, Rymarski Z and Oliwa W 2021 Gathering energy of the stray currents in electrified railways environment for power supply *Energies* **14** 6206

[4] Aatif S, Hu H, Rafiq F and He Z 2021 Analysis of rail potential and stray current in MVDC railway electrification system *Railw. Eng. Sci.* **29** 394–407

[5] Höger M, Regula M and Roch M 2023 Investigating the impacts of high voltage powerlines on ground current fields *Transp. Res. Proc.* **74** 900–7

[6] Mariscotti A 2020 Stray current protection and monitoring systems: characteristic quantities, assessment of performance and verification *Sensors* **20** 6610

[7] Charalambous C A, Cotton I and Aylott P 2008 A simulation tool to predict the impact of soil topologies on coupling between a light rail system and buried third-party infrastructure *IEEE Trans. Veh. Technol.* **57** 1404–16

[8] Chen L, Zhang B, Wei K, Fang D and Zou Q 2021 Analysis of leakage current characteristics of rail insulation fasteners based on ANSYS *2021 IEEE Sustainable Power and Energy Conf. (Ispec), (Nanjing, China)* pp 2640–3

[9] Zaboli A, Vahidi B, Yousefi S and Hosseini-biyouki M M 2017 Evaluation and control of stray current in dc-electrified railway systems *IEEE Trans. Veh. Technol.* **66** 974–80

[10] Huang K, Lin G and Liu Z 2022 Prediction approach of negative rail potentials and stray currents in medium-low-speed maglev *IEEE Trans. Transp. Electrif.* **8** 3801–15

[11] Liu W, Li T, Zheng J, Pan W and Yin Y 2021 Evaluation of the effect of stray current collection system in DC-electrified railway system *IEEE Trans. Veh. Technol.* **70** 6542–53

[12] Zhu C *et al* 2020 Simulation method of DC traction power systems with complex operation conditions based on unified chain model *2020 IEEE 9th Int. Power Electronics and Motion Control Conf. (IPEMC2020-ECCE Asia), (Nanjing, China)* pp 846–52

[13] Jamali S, Alamuti M M and Savaghebi M 2008 Effects of different earthing schemes on the stray current in rail transit systems *2008 43rd Int. Universities Power Engineering Conf. (Padua, Italy)* pp 1–5

[14] Fichera F, Mariscotti A, Ogunsola A and Sandrolini L 2013 Comparison of distributed and lumped parameters stray current models *2013 Africon, Pointe aux Piments, Mauritius* pp 1–5

[15] Li C, Du Q, Guo Y, Liu Y, Yang F, Chen L, Zhang X, Huang G, Gao G and Wu G 2023 Modeling of stray currents from metro intruding into power system considering the complex geological conditions in modern megacities *IEEE Trans. Transp. Electrif.* **9** 1653–63

[16] Tang M *et al* 2023 The distribution analysis of the ground potential and stray current in power grid under the operation of metro system *2023 2nd Int. Conf. on Power Systems and Electrical Technology (PSET) (Milan, Italy)* pp 158–62

[17] Zhou Q, Lin S, Lin X and Wang A 2022 A uniform model for stray current of long-line DC metro systems *IEEE Trans. Transp. Electrif.* **8** 2915–27

[18] Olivieri C, Di Leonardo L, de Paulis F, Orlandi A, Sbarra F and Camomilla M 2025 Experimentally-based circuit modeling validation of a dc-electrified railway system for rail voltage and stray-current evaluation *Electronics* **14** 4541

[19] Paul C R 1994 *Analysis of Multiconductor Transmission Lines* (Wiley)

[20] Analog Devices LTspice (available at: www.analog.com/en/design-center/design-tools-and-calculators/ltspice-simulator.html) (Accessed 11 March 2026) LTspice

[21] Ogunsola A, Mariscotti A and Sandrolini L 2012 Estimation of stray current from a DC-electrified railway and impressed potential on a buried pipe *IEEE Trans. Power Deliv.* **27** 2238–46

[22] Song R, Xia Y and Du S 2023 Dynamic analysis and modeling of the natural gas pipeline using the electrical analogy *2023 IEEE Power & Energy Society General Meeting (PESGM) (Orlando, FL, USA)* pp 1–5

[23] Zhang J 2024 Study on the corrosion of DC stray current to the horizontal buried angle of buried metal *2024 11th Int. Forum on Electrical Engineering and Automation (IFEEA)* pp 136–9

[24] Vlach J, Singhal K and Ed I I 1994 *Computer Methods for Circuit Analysis and Design* (Van Nostrand Reinhold)